Highly Sensitive Electromechanical Piezoresistive Pressure Sensors Based on Large-Area Layered PtSe2 Films

Wagner, S.; Yim, C.; Mcevoy, N.; Kataria, S.; Yokaribas, V.; Kuc, A. B.; Pindl, S.; Fritzen, C.-P.; Heine, T.; Duesberg, G. S.; Lemme, M. C.;

Communication

Highly sensitive electromechanical piezoresistive pressure sensors based on large-area layered PtSe2 films

Stefan Wagner, Chanyoung Yim, Niall McEvoy, Satender Kataria, Volkan Yokaribas, Agnieszka Kuc, Stephan Pindl, Claus-Peter Fritzen, Thomas Heine, Georg S. Duesberg, and Max C. Lemme

Just Accepted

Highly sensitive electromechanical piezoresistive pressure sensors based on large-area layered PtSe₂ films

Stefan Wagner[1], Chanyoung Yim[2], Niall McEvoy[3], Satender Kataria[1], Volkan Yokaribas[4], Agnieszka Kuc[5,8], Stephan Pindl[6], Claus-Peter Fritzen[4], Thomas Heine[5,7,8], Georg S. Duesberg[3], Max C. Lemme[1,9]*

[1]Chair of Electronic Devices, Faculty of Electrical Engineering and Information Technology, RWTH Aachen University, Otto-Blumenthal-Str. 2, 52074 Aachen, Germany

[2]Institute of Physics, EIT 2, Faculty of Electrical Engineering and Information Technology, Universität der Bundeswehr München, Werner-Heisenberg-Weg 39, 85577 Neubiberg, Germany

[3]Centre for Research on Adaptive Nanostructures and Nanodevices (CRANN), Advanced Materials and BioEngineering Research (AMBER) and School of Chemistry, Trinity College Dublin, Dublin 2, Ireland

[4]Department of Mechanical Engineering, University of Siegen, 57076 Siegen, Germany

[5]Wilhelm-Ostwald-Institut für Physikalische und Theoretische Chemie, Universität Leipzig, Linné Str. 2, 04103 Leipzig, Germany

[6]Infineon Technologies AG, Wernerwerkstraße 2, 93049 Regensburg, Germany

[7]Theoretical Chemistry, TU Dresden, 01062 Dresden, Germany

[8]Helmholtz Center Dresden-Rossendorf, Institute of Resource Ecology, 01328 Dresden

[9]AMO GmbH, Advanced Microelectronic Center Aachen (AMICA), Otto-Blumenthal-Str. 25,

52074 Aachen, Germany

ABSTRACT: Two-dimensional (2D) layered materials are ideal for micro- and nanoelectromechanical systems (MEMS/NEMS) due to their ultimate thinness. Platinum diselenide (PtSe$_2$), an exciting and unexplored 2D transition metal dichalcogenides (TMD) material, is particularly interesting because its low temperature growth process is scalable and compatible with silicon technology. Here, we report the potential of thin PtSe$_2$ films as electromechanical piezoresistive sensors. All experiments have been conducted with semi-metallic PtSe$_2$ films grown by thermally assisted conversion of platinum at a CMOS-compatible temperature of 400°C. We report high negative gauge factors of up to -84.8 obtained experimentally from PtSe$_2$ strain gauges in a bending cantilever beam setup. Integrated NEMS piezoresistive pressure sensors with freestanding PMMA/PtSe$_2$ membranes confirm the negative gauge factor and exhibit very high sensitivity, outperforming previously reported values by orders of magnitude. We employ density functional theory (DFT) calculations to understand the origin of the measured negative gauge factor. Our results suggest PtSe$_2$ as a very promising candidate for future NEMS applications, including integration into CMOS production lines.

Layered two-dimensional (2D) materials have extraordinary electrical, optical and mechanical properties that suggest high potential for a wide range of nanoelectronics applications.[1,2] 2D transition metal dichalcogenides (TMDs) have recently been intensively investigated due to their wide range of inherent electronic properties that complement graphene. Out of this family, platinum diselenide ($PtSe_2$) is a relatively new and thus little explored TMD material. Monolayer $PtSe_2$ is a semiconductor with a band gap of 1.2 eV,[3] while bulk $PtSe_2$ becomes semi-metallic with zero band gap.[4,5] It has been grown epitaxially[6] or synthesized on insulating substrates using thermally assisted conversion (TAC) of predeposited platinum (Pt) films by a vaporized solid selenium precursor.[4,7] The latter process can be carried out at temperatures between 400 °C and 450 °C, which is compatible with standard semiconductor back end of line (BEOL) processing,[8] in contrast to other 2D materials.[9–11] We have demonstrated potential applications of TAC $PtSe_2$ in highly sensitive gas sensors and photodetectors with equal or even superior performance compared to graphene and other TMD-based devices.[7,12] Furthermore, top-down structured electrical devices with $PtSe_2$ have been demonstrated.[13] Here, we explore the electromechanical properties of $PtSe_2$ in nanoelectromechanical (NEMS) pressure sensors. The devices utilize the piezoresistive effect in $PtSe_2$, which gives rise to a change in its electrical resistance upon mechanical strain. We investigate $PtSe_2$-membrane based pressure sensors and find sensitivities that are orders of magnitude higher than those of nanomaterial-based devices,[14–17] including graphene.[18–20] Furthermore, we obtain an average negative gauge factor (GF) of -84.8 for $PtSe_2$ from a bending beam setup. Detailed density functional theory (DFT) simulations reveal an increase in the density of states (DOS) at the Fermi level of bulk $PtSe_2$, corroborating the experimentally observed piezoresistive properties.

Polycrystalline PtSe$_2$ films with nanometer sized grains were grown on silicon/silicon dioxide

(Si/SiO$_2$) substrates by TAC at 400 °C of predeposited 1 nm thick Pt films (Figure S1 in the

supporting information). Comprehensive characterization of layered PtSe$_2$ thin films synthesized

in this manner, including X-ray photoelectron spectroscopy and scanning transmission electron

microscopy is presented in our previous work.[4,7] The thickness and roughness of the layers was

determined by atomic force microscopy (AFM, Figure 1a,b). A thickness of 4.5 nm was found

for the selenized 1 nm initial Pt film. Assuming an interlayer distance of 0.6 nm for PtSe$_2$,[21] this

corresponds to 7-8 layers for the 4.5 nm thick PtSe$_2$ film. The root mean square (RMS)

roughness of the layer was 0.284 nm. The Raman spectrum of the PtSe$_2$ film shows two sharp

and prominent peaks corresponding to the E$_g$ and A$_{1g}$ modes of the 1T phase, attesting the

crystalline nature of the films (Figure 1c).[4] After the film growth, a polymethyl metacrylate

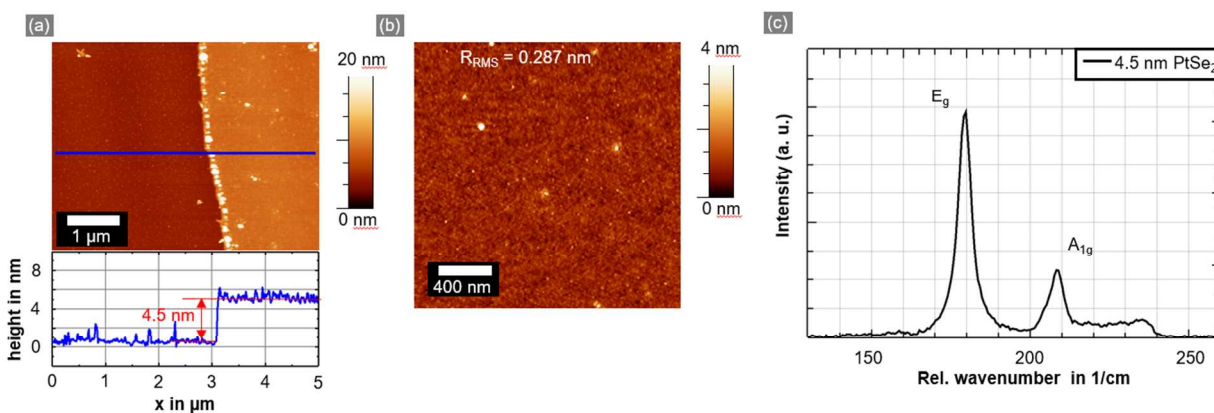(PMMA) was spin-coated on top of the PtSe$_2$.

Figure 1. As-grown PtSe$_2$ film characterization: (a) AFM measurement of the selenized 1 nm

initial Pt film including height profile of the step between the Si/SiO$_2$ substrate to the PtSe$_2$ film;

(b) High-resolution AFM measurement displaying the RMS roughness; (c) Raman spectrum of

the as-grown 4.5 nm thick PtSe$_2$ sample.

These centimeter-scale $PtSe_2$ thin films were transferred onto the substrate comprising of 79 independent pressure devices, using a typical polymer supported transfer process as described for graphene.[22] Each device consists of cavities covered by a patterned $PtSe_2$ film located in between metal contacts (Figure 2a-c). The PMMA layer was not removed after the transfer in order to stabilize and protect the $PtSe_2$ layer against environmental influences and to reduce possible cross sensitivity of the sensor. Details of the fabrication processes are described in the Experimental section and in the supporting information Figure S2a-d. A non-invasive Raman tomography cross-section, as demonstrated recently for graphene membranes,[23] confirms the presence of free-standing $PtSe_2$ across the cavity (Figure 2d,e) where devices with suspended $PtSe_2$ (Figure 2e, top) and collapsed membrane (Figure 2e, bottom) were measured and can clearly be distinguished with this method. The corresponding spectrum of the suspended $PtSe_2$ shows the characteristic E_g and A_{1g} modes without the Si(I) peak (Figure 2d, top), whereas the spectrum taken at the bottom of the trench shows only the characteristic Si(I) peak of the Si substrate (Figure 2d, bottom). This clear separation is feasible due to the 1.4 μm deep cavity, which defines the distance between the suspended $PtSe_2$ and the Si substrate.

The operation of the investigated pressure sensors can be described in the following way: the $PtSe_2$/PMMA membranes seal the cavities and trap environmental pressure inside them.[24–26] A different pressure (lower or higher) outside the cavity leads to a deflection of the $PtSe_2$ membrane. This deflection induces strain in the $PtSe_2$ layer, resulting in a change of its resistance. The chip design used in the present experiments includes devices of similar size without cavities as control references. The pressure sensors, after wire-bonding and packaging into a chip socket, were placed in a home-built pressure chamber where pressure can be regulated from 1000 mbar (environmental pressure) down to 200 mbar (supporting information

Figure S3). The pressure, humidity and temperature inside the chamber are recorded and controlled with commercial sensors during the experiments. Argon (Ar) atmosphere was used to exclude cross-sensitivity effects with gases and/or humidity.[7] The current-voltage (I-V) characteristics of the $PtSe_2$ device for environmental pressure shows good linearity, i.e. the transferred $PtSe_2$ forms good Ohmic contacts with metal (gold) electrodes (supporting information Figure S4). The measured data is presented in Figure 2f along with the simultaneously measured pressure (dashed red line, right y-axis). The resistance across the $PtSe_2$ sensors decreases with applied increasing strain on the membrane (caused by the decrease in pressure, supporting information Figure S5a). A pressure difference of 800 mbar between the outside and the inside of the cavity leads roughly to 7% of change in resistance.
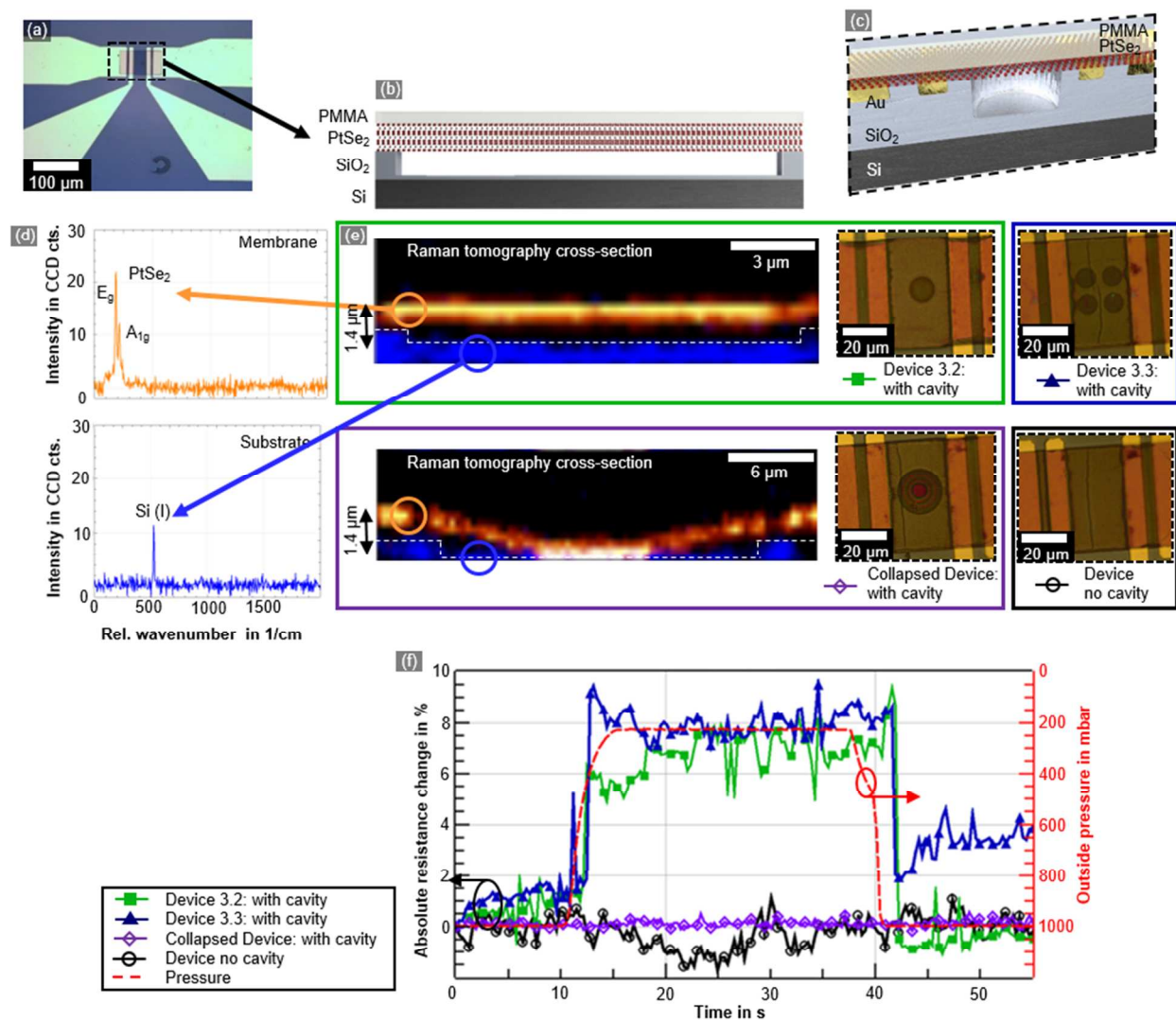
Figure 2. Pressure sensor fabrication and measurement. (a) Optical micrograph of one device with Au contacts and the PtSe$_2$ channel across the cavity area. (b) Schematic cross-section of the cavity area with suspended PtSe$_2$. (c) Schematic of one device including contacts and cavity area. (d) Raman point spectrum of the PtSe$_2$ membrane area and the Si substrate. (e) Raman tomography cross-sections of one device with suspended PtSe$_2$ (device 3.2) and one with collapsed membrane (Collapsed Device). On the right are the corresponding optical micrographs of the cavity areas (device 3.2 and the collapsed device) as well as one other working device (device 3.3) and one device without cavity (device no cavity) as reference. (f) Resistance change

in % for one pressure cycle (vented, pumped down to 200 mbar, vented) of the four devices shown in (e) (left y-axis) and pressure on the outside of the membrane (right y-axis).

The results of four devices are displayed in Figure 2f: two intact membranes on cavities (filled green squares and filled blue triangles), one with a collapsed membrane (empty purple diamond) and one device without cavity for reference (empty black circles). A slight decrease (increase) in humidity during evacuation (venting) of the chamber is commonly observed for all measurements (supporting information Figure S5b), but does not give rise to changes in the resistance. Cross-sensitivity towards humidity can thus be excluded from having any substantial influence on the device behavior. We conclude that the observed resistance change is primarily caused by pressure (i.e. strain) changes during the measurements.

The absolute sensitivity (S) of a piezoresistive device is calculated using equation (1), where $ΔR/R$ is the absolute value of the relative resistance change and $ΔP$ is the pressure change during the sensor operation.[18]

$$S = \frac{ΔR}{R \cdot ΔP} \tag{1}$$

A total of 19 working devices were measured on four different chips through 69 different measurements (Figure 3a). A sensitivity of $1.05 \times 10^{-4}\,\text{mbar}^{-1}$ was extracted from Figure 2f. An average of $5.51 \times 10^{-4}\,\text{mbar}^{-1}$ was calculated for all measured devices (best device not included). The results were compared to some other NEMS pressure sensors which operate in a similar pressure range (Figure 3b,c). These use gallium arsenide (GaAs),[27] Si nanowires (Si NWs),[15,16] single- and multi-wall carbon nanotubes (SWNT and MWNT)[14,17] and graphene[18–20] as the piezoresistive materials. However, for most of these (except Smith et al.[18] and Fung et al.[17]) a separate membrane is needed which is treated, or where the piezoresistive materials are grown or

applied, in a separate fabrication step. This adds additional complexity to the fabrication process, which is not the case for the $PtSe_2$-based pressure sensors, because the material acts as membrane and sensor at the same time. The thickness of other material is limited due to their mechanical stability. The measured sensitivity outperforms the best reported 2D and low dimensional materials based pressure sensors by a factor between 3 and 70 (Figure 3b). The SWNT-based pressure sensor[14] shows an equal sensitivity, however the membrane areas are nearly two to four orders of magnitude larger than the $PtSe_2$ membrane. To take this into account the sensitivity can be normalized to the membrane area to receive a direct comparison between the devices independent of their membrane size.[28,18] Here, the $PtSe_2$-based pressure sensor shows nearly 2 to 5 orders of magnitude higher sensitivity than the other devices (Figure 3c, see also supporting information Table S6).

We further point out that one of the devices showed an exceptionally high sensitivity of $1.64 \times 10^{-3}\,mbar^{-1}$ (Figure S5c). Even though it could not be reproduced in other devices, this value was repeatedly measured for that particular device (Figure 3a, device 2.1). The sensitivity and normalized sensitivity of this device are plotted in Figure 3b,c (black star). When normalized to the membrane area, this device is over 3 orders of magnitude more sensitive than the highest performing devices shown in Figure 3c (a SWNT[14] and a graphene membrane[18] based device), and 4 to 6 orders of magnitude more sensitive than other reported devices.
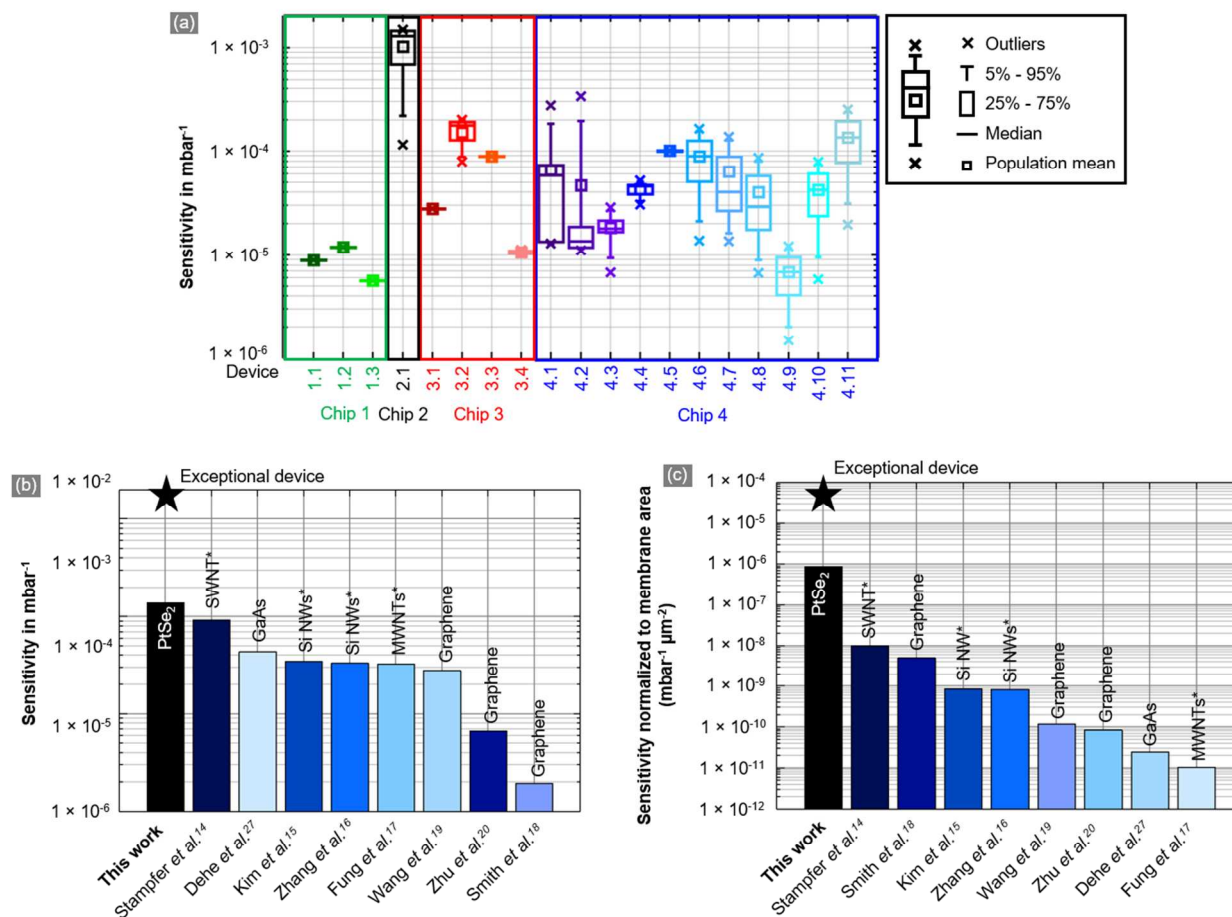
Figure 3. Comparison of all measured chips and devices as well as comparison of various pressure sensor devices using different materials for piezoresistive detection. (a) Box and whiskers plot of all measured chips, devices and repeated measurements; (b) Comparison of the sensitivity in mbar-1 with other pressure sensors; (c) comparison of the sensitivity normalized by membrane area in mbar^{-1} μm^{-2} with other pressure sensors. In plots (b) and (c), devices which require a separate membrane are indicated with a * and the device with exceptionally high sensitivity is indicated by a black star.

A bending beam setup was used to measure the piezoresistive gauge factor of the 4.5 nm and 9 nm thick PtS_2 films, which consisted of 7 to 8 and approximately 15 layers, respectively. The

bending beam setup enables measurements of well-defined strain fields in a very simple way (for

details see supporting information). The gauge factor (GF) can be extracted using equation (2).[29]

$$GF = \frac{\Delta R}{R_0 \cdot \varepsilon} \qquad (2)$$

Here, ε is the strain in the bending beam at the position of the sensor ($\varepsilon = 0.04\%$). A negative

gauge factor (GF) of -84.8 was obtained (Figure 4a, supporting information section S7 and S9).

The measured resistance change is shown in Figure 4b and in the supporting information Figure

S9b for two $PtSe_2$ layer thicknesses and masses of 2 kg and 0.5 kg (Figure S9c in the supporting

information). A measurement of multiple strain cycles with a mass of 2 kg is shown in Figure

S9d in the supporting information. In some measurements, the resistance did not immediately

return completely to its initial values after removing the mass (Figure 4b, 4.5 nm $PtSe_2$ device,

Figure S9b, d in the supporting information). This may be attributed to slip of the device or the

electrical contacts during measurements due to non-optimal adhesion to the beam. Furthermore,

a slight overshoot followed by oscillations was observed for some devices right after applying

the mass. These may be interpreted as natural oscillations due to the manual application of the

mass on the beam. Data from a commercially available metal strain gauge is used as a reference

(Figure 4b). A decrease in resistance with increasing strain on the $PtSe_2$ film corroborates the

integrated pressure sensor measurements (supporting information Figure S9a). The GF of the

$PtSe_2$ films exceeds the GF of the metal strain gauge (GF of 2)[29] and of graphene (GF of 2-

6).[24,30,31] While similar or higher GF have been found for doped silicon (GF of -100 to +200)[29] or

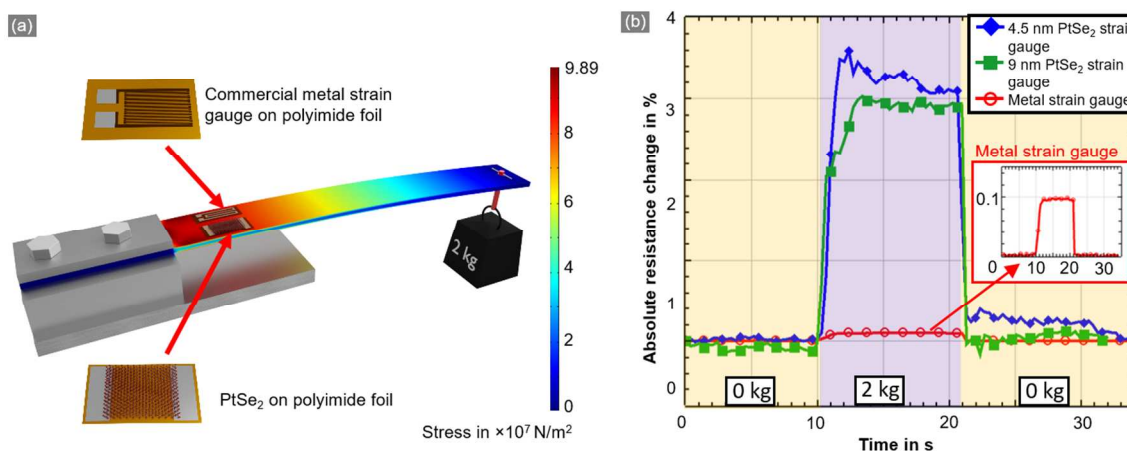mono- and trilayer MoS_2 (GF of -148 and -43.5).[32]

Figure 4. (a) Bending beam setup (cantilever beam) with applied PtSe$_2$ and commercially available metal strain gauges including stress simulation with the applied weight; (b) Electrical readout signal during the measurement with an absolute resistance change against time showing two PtSe$_2$ devices (of 4.5 nm PtSe$_2$, diamonds filled in blue and 9 nm PtSe$_2$, squares filled in green) and a metal strain gauge (empty red circles) as reference with an enlarged view in the inset.

DFT calculations were conducted to gain insights into the observed resistance decrease with increased strain in PtSe$_2$ films. The model was designed to represent the membrane covering the cavities of the PtSe$_2$ pressure sensors. Here, the deformation can be thought of as bi-axial strain acting on the PtSe$_2$ membrane. The model was fully optimized in terms of the lattice vectors and atomic positions. In the bulk system, which is similar to the experimental conditions in this work, biaxial strain means that the layers are stretched or compressed in plane. As bulk PtSe$_2$ is metallic, the density of states (DOS) at the Fermi level is found to increase under biaxial tensile strain (ε_a) and reduces under compression, as shown in the supporting information Figure S10a. This result is in accordance with the experimental findings, where the resistivity decreases with increased ε_a.

Next, we have considered the effect of the interlayer strain and compression (ε_c) on the DOS. The results are shown in the supporting information Figure S10b. The compression of the interlayer distance has the opposite influence on the system and it slightly reduces the DOS at the Fermi level. Finally, we have considered the two effects acting in tandem in the following way: for in-plane stretching, there is compression out of the plane, and vice versa (Figure 5a). The results for the combined effect are shown in Figure 5b. Once again, the DOS at the Fermi level is increased for the in plane stretching and compression in the out-of-plane direction. However, the effect is reduced compared to just ε_a, due to the opposite effect of the interlayer compression, as shown in the supporting information Figure S10b. In comparison to the significant increase of the DOS at the Fermi level upon strain the band structure shows only minor changes (Figure S10c in the supporting information) not indicating strong differences in the effective masses under strain.
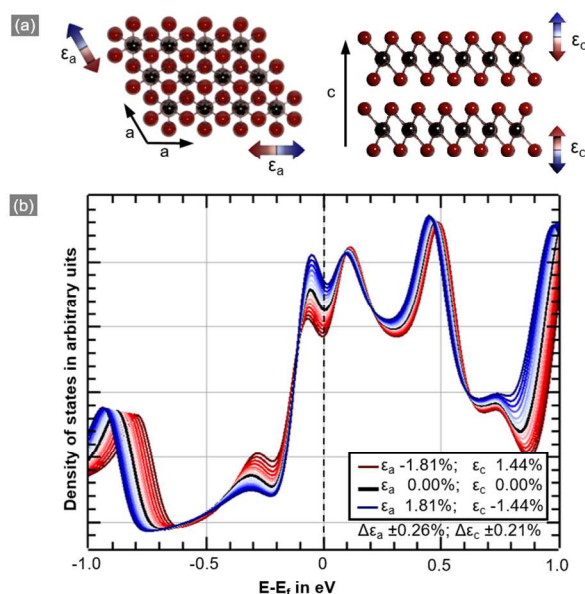
Figure 5. (a) Top and side view of the PtSe$_2$ bulk shown with the in-plane, a and out-of-plane, c lattice vectors, and the direction of the applied strain (ε_a and ε_c). (b) Density of states close to the Fermi level (shifted to zero) under applied tensile strain and compression.

An increase in DOS has also been reported for other single and few layer semiconducting TMDs, like MoS$_2$,[33] MoSe$_2$,[34] WSe$_2$[34] and also PtSe$_2$.[35] The semiconducting materials exhibit a decrease in band gap and even a transition to metallic behavior with applied strain, resulting in a negative gauge factor. For more detailed future studies the influence of many other parameters should be considered and investigated, including the adhesive interface between the steel beam and the polyimide foil, the thickness and mechanical properties of the foil and the PMMA layer covering the PtSe$_2$. Also, the crystallographic orientations, thickness and other material properties of the TAC-grown PtSe$_2$ film need to be investigated and considered in the simulations. Nevertheless, the results of the simulations show a clear indication of an increase in DOS, leading to a decrease in resistance under the applied strain, which is the most plausible cause of the experimentally extracted negative GF.

We have demonstrated $PtSe_2$-based piezoresistive pressure sensors with high gauge factors and very high sensitivity. The experiments were conducted on large-area $PtSe_2$ thin films grown by a scalable method of thermal conversion of metallic films at a low temperature of 400°C. A negative gauge factor of approximately -85 was obtained from a $PtSe_2$ strain gauge through bending beam experiments and can be understood in terms of a strain-induced increase in the DOS, as verified through DFT simulations. Furthermore, integrated piezoresistive pressure sensors were fabricated using $PtSe_2$/PMMA membranes. The $PtSe_2$ pressure sensors showed very high sensitivity, outperforming piezoresistive pressure sensors based on other materials by at least a factor of 82. When normalized to the active membrane area, the sensitivity of our devices is almost two to five orders of magnitude larger than values reported for any other technology to date. One exceptional device has an even higher sensitivity of 1.64×10^{-3} mbar^{-1} and outperforms existing technologies by an even greater margin. These results suggest that layered 2D $PtSe_2$ has great potential for future piezoresistive NEMS applications, beyond the demonstrated pressure sensors. These devices have a footprint that is up to four orders of magnitude smaller than other pressure sensors while showing a similar or even higher sensitivity. Further down-scaling to smaller cavities will improve the stability and yield of the membranes, and allow decreasing the membrane thickness to maintain the high sensitivity. The low growth temperature and general CMOS material compatibility makes $PtSe_2$ highly attractive for future silicon technology integration.

Methods

Materials Synthesis and analysis

Pt layers with a thickness of 1 and 2 nm were sputter deposited on 1.5 x 1.5 cm^2 Si/SiO$_2$ substrates using a Gatan coating system (Gatan 682 PECS) with a 19 mm diameter Pt target. A TAC process was used to selenize the pre-deposited Pt layers, as described in detail in references.[4,7] The cross-sectional Raman measurements were conducted using a WITec alpha 300R system with a 532 nm laser as source of excitation. A laser power of 75 µW was used. For obtaining single Raman spectra an 1800 g/mm grating was used, while the depth scan (cross-section) was conducted with a 300 g/mm grating. The system is limited to a lateral and vertical resolution of 300 nm and 900 nm, respectively.

Strain gauge fabrication

The strain gauges were fabricated by transferring as-grown PtSe$_2$ films onto pre-patterned polyimide foil substrates. A typical polymer-supported transfer method was used for the film transfer. 200 nm thick PMMA (Allresist AR-P 649.04) was spun on the as-grown PtSe$_2$ samples at a speed of 2000 rpm for 50 s. After spin-coating, the samples were annealed for 5 min at 80°C to cure the PMMA. 2 molar KOH was used to etch away the SiO$_2$ layer and release the PMMA-covered PtSe$_2$ films from the substrate. The PMMA-covered PtSe$_2$ films were cleaned in DI-water, followed by a transfer to the pre-patterned (500 nm thick copper contacts from evaporation) polyimide foil. After drying, the foil was glued (super glue Z70 by HBM) onto the steel beam (size of 300×30 mm^2, 3 mm thick), 200 mm away from the loading point. A commercially available metal strain gauge was glued next to the PtSe$_2$ strain gauge. Cables were then soldered onto the contact pads for electrical connections.

Pressure sensor fabrication

A Si chip (7×7 mm^2) with 1.6 µm thick SiO_2 was used as a device substrate (Figure S2a in the supporting information). The cavities have circular geometry (radii between 2 µm and 20 µm) with arrays of 1 to 15 cavities and rectangular geometries (length of 20 µm and width between 2 µm and 4 µm) in arrays between 1 and 3 cavities. They were structured by photolithography, followed by Ar- and CHF_3-based reactive ion etching (RIE, 200 mW, 40 mTorr) to create a vertical profile with 1.4 µm of depth (Figure S2b in the supporting information). The contact regions were defined by photolithography, followed by a RIE process to embed the contacts and self-aligned metal evaporation (Cr/Au, 40 nm/400 nm, Figure S2c in the supporting information). The $PtSe_2$ films grown from 1 nm initial Pt films were transferred onto the device substrate using a PMMA-supported transport method as described above (Figure S2d in the supporting information). Lastly, the chip was wire bonded into a 44-pin PLCC chip package using 25 µm diameter Au wire.

Simulation

All calculations were performed using the DFT method as implemented in the VASP plane wave code.[36,37] Ion-electron interactions were described by projector augmented wave approximation.[38] We have employed Perdew–Burke–Ernzerhof (PBE)[39] functional under the generalized gradient approximation. Van der Waals interaction corrections were included using the D3 approach proposed by Grimme.[40] Cutoff energy was set to 600 eV and the convergence threshold for residual force was 0.01 eV Å^{-1}. Brillouin zone integration was carried out at $6\times6\times6$

Monkhorst–Pack k-grids. Spin-orbit coupling (SOC) was included in the electronic structure calculations. Bulk $PtSe_2$ was fully optimized (lattice vectors and atomic positions) resulting in the following lattice vectors: a = b = 3.788 Å and c = 4.790 Å, and a distance between Se atoms in the Se-Pt-Se sandwich of 2.550 Å. This is in good agreement with the experimental data by Wang et al.,[6] with a = b = 3.70 Å and the distance between Se atoms of 2.53 Å.

1
2
3
4
5
6
7
8
9
10
11
12
13
14
15
16
17
18
19
20
21
22
23
24
25
26
27
28
29
30
31
32
33
34
35
36
37
38
39
40
41
42
43
44
45
46
47
48
49
50
51
52
53
54
55
56
57
58
59
60

ASSOCIATED CONTENT

Supporting Information

Schematic of the growth of $PtSe_2$ with additional Raman spectra. The fabrication process is described in a schematic and the measurement chamber is shown on a schematic. I-V characteristic of the unstrained pressure device is shown as well as some additional electrical characterization data of the pressure devices. A table of the compared pressure sensors from literature is shown. The strain gauge measurements are described in detail, including the I-V characteristic of the device as well as some further electrical measured data. Further DFT calculations are shown for bulk and for three layer $PtSe_2$. (PDF)

AUTHOR INFORMATION

Corresponding Author

*Tel: +49 241 8867 200, Email: max.lemme@eld.rwth-aachen.de; lemme@amo.de

Author Contributions

The manuscript was written through contributions of all authors. All authors have given approval to the final version of the manuscript.

15/SIRG/3329) and the German Research Foundation (DFG LE 2440/1-2 and HE 3543/18-1) are

gratefully acknowledged.

ABBREVIATIONS

2D, two dimensional; $PtSe_2$, Platinum diselenide; TMD, transition metal dichalcogenides;

MEMS, microelectromechanical systems; NEMS, nanoelectromechanical systems; DFT, density

function theory; TAC, thermally assisted conversion; Pt, Platinum; GF, gauge factor; DOS,

density of states; Si, silicon; SiO_2, silicon oxide; AFM, atomic force microscopy; RMS, root

mean square; PMMA, polymethyl metacrylate; Ar, argon; I-V , current-voltage; GaAs, gallium

arsenide; Si NW, silicon nanowire; SWNT, single wall nanotube; MWNT, multi wall nanotube.

1
2
3
4
5
6
7
8
9
10
11
12
13
14
15
16
17
18
19
20
21
22
23
24
25
26
27
28
29
30
31
32
33
34
35
36
37
38
39
40
41
42
43
44
45
46
47
48
49
50
51
52
53
54
55
56
57
58
59
60

REFERENCES

(1)   Lemme, M. C.; Li, L.-J.; Palacios, T.; Schwierz, F. Two-Dimensional Materials for
       Electronic Applications. *MRS Bull.* **2014**.

(2)   Gupta, A.; Sakthivel, T.; Seal, S. Recent Development in 2D Materials beyond Graphene.
       Prog. Mater. Sci. **2015**.

(3)   Wang, Y.; Li, L.; Yao, W.; Song, S.; Sun, J. T.; Pan, J.; Ren, X.; Li, C.; Okunishi, E.;
       Wang, Y.-Q.; et al. Monolayer PtSe2, a New Semiconducting Transition-Metal-
       Dichalcogenide, Epitaxially Grown by Direct Selenization of Pt. *Nano Lett.* **2015**.

(4)   O'Brien, M.; McEvoy, N.; Motta, C.; Zheng, J.-Y.; Berner, N. C.; Kotakoski, J.; Kenan
       Elibol; Pennycook, T. J.; Meyer, J. C.; Yim, C.; et al. Raman Characterization of Platinum
       Diselenide Thin Films. *2D Mater.* **2016**.

(5)   Zhang, W.; Qin, J.; Huang, Z.; Zhang, W. The Mechanism of Layer Number and Strain
       Dependent Bandgap of 2D Crystal PtSe2. *J. Appl. Phys.* **2017**.

(6)   Wang, Y.; Li, L.; Yao, W.; Song, S.; Sun, J. T.; Pan, J.; Ren, X.; Li, C.; Okunishi, E.;
       Wang, Y.-Q.; et al. Monolayer PtSe2, a New Semiconducting Transition-Metal-
       Dichalcogenide, Epitaxially Grown by Direct Selenization of Pt. *Nano Lett.* **2015**.

(7)   Yim, C.; Lee, K.; McEvoy, N.; O'Brien, M.; Riazimehr, S.; Berner, N. C.; Cullen, C. P.;
       Kotakoski, J.; Meyer, J. C.; Lemme, M. C.; et al. High-Performance Hybrid Electronic
       Devices from Layered PtSe2 Films Grown at Low Temperature. *ACS Nano* **2016**.

(8)   Plummer, J. D. *Silicon VLSI Technology: Fundamentals, Practice, and Modeling*; Pearson
       Education India, **2009**.

(9)   Kataria, S.; Wagner, S.; Ruhkopf, J.; Gahoi, A.; Pandey, H.; Bornemann, R.; Vaziri, S.;
       Smith, A. D.; Ostling, M.; Lemme, M. C. Chemical Vapor Deposited Graphene: From
       Synthesis to Applications. *Phys. Status Solidi A* **2014**.

(10)   McCreary, K. M.; Hanbicki, A. T.; Jernigan, G. G.; Culbertson, J. C.; Jonker, B. T.
       Synthesis of Large-Area WS$_2$ Monolayers with Exceptional Photoluminescence. *Sci. Rep.*
       2016.

(11)   Kataria, S.; Wagner, S.; Cusati, T.; Fortunelli, A.; Iannaccone, G.; Pandey, H.; Fiori, G.;
       Lemme, M. C. Growth-Induced Strain in Chemical Vapor Deposited Monolayer MoS2:
       Experimental and Theoretical Investigation. *Adv. Mater. Interfaces* **2017**.

(12)   Yim, C.; McEvoy, N.; Riazimehr, S.; Schneider, D. S.; Gity, F.; Monaghan, S.; Hurley, P.
       K.; Lemme, M. C.; Duesberg, G. S. Wide Spectral Photoresponse of Layered Platinum
       Diselenide-Based Photodiodes. *Nano Lett.* **2018**.

(13)   Yim, C.; Passi, V.; Lemme, M. C.; Duesberg, G. S.; Coileáin, C. Ó.; Pallecchi, E.; Fadil,
       D.; McEvoy, N. Electrical Devices from Top-down Structured Platinum Diselenide Films.
       Npj 2D Mater. Appl. **2018**.

(14)   Stampfer, C.; Helbling, T.; Obergfell, D.; Schöberle, B.; Tripp, M. K.; Jungen, A.; Roth,
       S.; Bright, V. M.; Hierold, C. Fabrication of Single-Walled Carbon-Nanotube-Based
       Pressure Sensors. *Nano Lett.* **2006**.

(15)   Kim, J. H.; Park, K. T.; Kim, H. C.; Chun, K. Fabrication of a Piezoresistive Pressure
       Sensor for Enhancing Sensitivity Using Silicon Nanowire. In *TRANSDUCERS 2009 -
       2009 International Solid-State Sensors, Actuators and Microsystems Conference*; **2009**.

(16)   Zhang, J.; Zhao, Y.; Ge, Y.; Li, M.; Yang, L.; Mao, X. Design Optimization and
       Fabrication of High-Sensitivity SOI Pressure Sensors with High Signal-to-Noise Ratios
       Based on Silicon Nanowire Piezoresistors. *Micromachines* **2016**.

(17) Fung, C. K. M.; Zhang, M. Q. H.; Chan, R. H. M.; Li, W. J. A PMMA-Based Micro Pressure Sensor Chip Using Carbon Nanotubes as Sensing Elements. In *18th IEEE International Conference on Micro Electro Mechanical Systems, 2005. MEMS 2005*; **2005**.

(18) Smith, A. D.; Niklaus, F.; Paussa, A.; Vaziri, S.; Fischer, A. C.; Sterner, M.; Forsberg, F.; Delin, A.; Esseni, D.; Palestri, P.; et al. Electromechanical Piezoresistive Sensing in Suspended Graphene Membranes. *Nano Lett.* **2013**.

(19) Wang, Q.; Hong, W.; Dong, L. Graphene "Microdrums" on a Freestanding Perforated Thin Membrane for High Sensitivity MEMS Pressure Sensors. *Nanoscale* **2016**.

(20) Zhu, S.-E.; Ghatkesar, M. K.; Zhang, C.; Janssen, G. C. a. M. Graphene Based Piezoresistive Pressure Sensor. *Appl. Phys. Lett.* **2013**.

(21) Yan, M.; Wang, E.; Zhou, X.; Zhang, G.; Zhang, H.; Zhang, K.; Yao, W.; Lu, N.; Shuzhen Yang; Wu, S.; et al. High Quality Atomically Thin PtSe 2 Films Grown by Molecular Beam Epitaxy. *2D Mater.* **2017**.

(22) Wagner, S.; Weisenstein, C.; Smith, A. D.; Östling, M.; Kataria, S.; Lemme, M. C. Graphene Transfer Methods for the Fabrication of Membrane-Based NEMS Devices. *Microelectron. Eng.* **2016**.

(23) Wagner, S.; Dieing, T.; Centeno, A.; Zurutuza, A.; Smith, A. D.; Östling, M.; Kataria, S.; Lemme, M. C. Noninvasive Scanning Raman Spectroscopy and Tomography for Graphene Membrane Characterization. *Nano Lett.* **2017**.

(24) Smith, A. D.; Niklaus, F.; Paussa, A.; Schröder, S.; Fischer, A. C.; Sterner, M.; Wagner, S.; Vaziri, S.; Forsberg, F.; Esseni, D.; et al. Piezoresistive Properties of Suspended Graphene Membranes under Uniaxial and Biaxial Strain in Nanoelectromechanical Pressure Sensors. *ACS Nano* **2016**.

(25) Bunch, J. S.; Verbridge, S. S.; Alden, J. S.; van der Zande, A. M.; Parpia, J. M.; Craighead, H. G.; McEuen, P. L. Impermeable Atomic Membranes from Graphene Sheets. *Nano Lett.* **2008**.

(26) Dolleman, R. J.; Cartamil-Bueno, S. J.; Zant, H. S. J. van der; Steeneken, P. G. Graphene Gas Osmometers. *2D Mater.* **2017**.

(27) Dehe, A.; Fricke, K.; Mutamba, K.; Hartnagel, H. L. A Piezoresistive GaAs Pressure Sensor with GaAs/AlGaAs Membrane Technology. *J. Micromechanics Microengineering* **1995.**

(28) Clark, S. K.; Wise, K. D. Pressure Sensitivity in Anisotropically Etched Thin-Diaphragm Pressure Sensors. *IEEE Trans. Electron Devices* **1979**.

(29) Window, A. L. *Strain Gauge Technology*; Elsevier Applied Science: London; New York, **1992**.

(30) Huang, M.; Pascal, T. A.; Kim, H.; Goddard, W. A.; Greer, J. R. Electronic−Mechanical Coupling in Graphene from in Situ Nanoindentation Experiments and Multiscale Atomistic Simulations. *Nano Lett.* **2011**.

(31) Lee, Y.; Bae, S.; Jang, H.; Jang, S.; Zhu, S.-E.; Sim, S. H.; Song, Y. I.; Hong, B. H.; Ahn, J.-H. Wafer-Scale Synthesis and Transfer of Graphene Films. *Nano Lett.* **2010**.

(32) Manzeli, S.; Allain, A.; Ghadimi, A.; Kis, A. Piezoresistivity and Strain-Induced Band Gap Tuning in Atomically Thin MoS2. *Nano Lett.* **2015**.

(33) Nayak, A. P.; Bhattacharyya, S.; Zhu, J.; Liu, J.; Wu, X.; Pandey, T.; Jin, C.; Singh, A. K.; Akinwande, D.; Lin, J.-F. Pressure-Induced Semiconducting to Metallic Transition in Multilayered Molybdenum Disulphide. *Nat. Commun.* **2014**.

(34)   Hosseini, M.; Elahi, M.; Pourfath, M.; Esseni, D. Very Large Strain Gauges Based on Single Layer MoSe2 and WSe2 for Sensing Applications. *Appl. Phys. Lett.* **2015**.

(35)   Li, P.; Li, L.; Zeng, X. C. Tuning the Electronic Properties of Monolayer and Bilayer PtSe2via Strain Engineering. *J. Mater. Chem. C* **2016**.

(36)   Kresse, G.; Furthmüller, J. Efficiency of Ab-Initio Total Energy Calculations for Metals and Semiconductors Using a Plane-Wave Basis Set. *Comput. Mater. Sci.* **1996.**

(37)   Kresse, G.; Furthmüller, J. Efficient Iterative Schemes for Ab Initio Total-Energy Calculations Using a Plane-Wave Basis Set. *Phys. Rev. B* **1996**.

(38)   Blöchl, P. E. Projector Augmented-Wave Method. *Phys. Rev. B* **1994**.

(39)   Perdew, J. P.; Burke, K.; Ernzerhof, M. Generalized Gradient Approximation Made Simple. *Phys. Rev. Lett.* **1996**.

(40)   Grimme, S.; Ehrlich, S.; Goerigk, L. Effect of the Damping Function in Dispersion Corrected Density Functional Theory. *J. Comput. Chem.* **2011**.

1
2
3
4
5
6
7
8
9
10
11
12
13
14
15
16
17
18
19
20
21
22
23
24
25
26
27
28
29
30
31
32
33
34
35
36
37
38
39
40
41
42
43
44
45
46
47
48
49
50
51
52
53
54
55
56
57
58
59
60

Table of Contents graphic: